Accepted manuscript doi:
10.1680/jgeot.23.00074

Accepted manuscript
As a service to our authors and readers, we are putting peer-reviewed accepted manuscripts (AM) online, in the Ahead of Print section of each journal web page, shortly after acceptance.

Disclaimer
The AM is yet to be copyedited and formatted in journal house style but can still be read and referenced by quoting its unique reference number, the digital object identifier (DOI). Once the AM has been typeset, an 'uncorrected proof' PDF will replace the 'accepted manuscript' PDF. These formatted articles may still be corrected by the authors. During the Production process, errors may be discovered which could affect the content, and all legal disclaimers that apply to the journal relate to these versions also.

Version of record
The final edited article will be published in PDF and HTML and will contain all author corrections and is considered the version of record. Authors wishing to reference an article published Ahead of Print should quote its DOI. When an issue becomes available, queuing Ahead of Print articles will move to that issue's Table of Contents. When the article is published in a journal issue, the full reference should be cited in addition to the DOI.

Accepted manuscript doi: 10.1680/jgeot.23.00074

Submitted: 24 March 2023

Published online in 'accepted manuscript' format: 9 August 2024

Manuscript title: The impact of thermal-hydraulic variation on tunnel long-term performance: a tale of two tunnels

Authors: Chao Wang*†, Zhipeng Xiao*‡, Vanessa Di Murro‡, John Osborne‡, Miles Friedman§ and Zili Li*†

Affiliations: *Civil, Structural and Environmental Engineering, University College Cork, Cork, Ireland †Irish Centre for Research in Applied Geosciences, University College Dublin, Ireland ‡European Centre for Nuclear Research, CERN, Geneva, Switzerland §Transport Infrastructure Ireland, Dublin, Ireland

Corresponding author: Zili Li, Civil, Structural and Environmental Engineering, University College Cork, Cork, Ireland and Irish Centre for Research in Applied Geosciences, University College Dublin, Ireland

E-mail: zili.li@ucc.ie; zilil.li@mit.edu

Accepted manuscript doi: 10.1680/jgeot.23.00074

Abstract
Long-term structural performance of ageing tunnels is influenced by various natural and anthropogenic factors. This study examines the impacts of two rarely-investigated climatic factors: rainfall and temperature. Two dedicated case studies were conducted on the CERN TT10 tunnel and Dublin Port Tunnel (DPT) using distributed fibre optic strain sensing (DFOS) and wireless sensor network (WSN) monitoring respectively. DFOS data showed an increasing deformation in TT10 tunnel, attributed to tunnel deteriorations and ground deformation, with seasonal variation of lining strains linked to rainfall-related seasonal change in pore water pressure. However, inconsistencies in rainfall-strain correlation were also noted due to geological complexities and varying pore water pressure sources. In contrast, WSN measurements showed that DPT deformation correlated with temperature, instead of precipitation. DPT deformation increased in warmer seasons and decreased in colder ones, in the absence of external disturbances, comprising reversible thermal deformation and irreversible deterioration-induced deformation. Over time, cyclic and periodic temperature changes caused elastic deformation to reverse, while plastic deformation accumulated, leading to ongoing tunnel deformation. These findings bring more insights into the resilience of critical underground infrastructure vulnerable to climate change, groundwater variations, and other environmental factors.

Keywords: temperature effect; rainfall effect; seasonable change; long-term tunnel performance; distributed fibre optic sensing; wireless sensor network

Accepted manuscript doi: 10.1680/jgeot.23.00074

Introduction

After construction, underground tunnels are influenced by various internal and external factors over their lifetime. These factors in the long run can bring about unfavourable functional and operational risks, such as excessive lining deformation and ground settlement (Manchao et al., 2015; Shi and Li, 2015), or cause tunnel instability, resulting in economic losses and casualties (Lü et al., 2018; Zhang et al., 2020a), as seen in the Saint Petersburg's subway damage (Hu et al., 2008). Previously, most investigations largely focused on external disturbances (e.g., adjacent construction) and/or internal deteriorations (e.g., hydraulic issues) affecting the long-term tunnel performance (Li et al., 2015; Liang et al., 2021; Liu et al., 2020; Meng et al., 2022; Showkati et al., 2021). However, there has been limited attention to the impact of climatic hydro-thermal factors, like significant rainfall and temperature variations, on the long-term behaviour of ageing tunnels.

Many tunnels, such as metro and utility tunnels, are constructed in congested urban areas and are subjected to various external disturbances, including adjacent excavations (Liang et al., 2021; Liu et al., 2020; Meng et al., 2022; Zheng et al., 2022), excessive surcharge (Huang and Zhang, 2016), and dewatering (Guo et al., 2021). Internal factors like lining deterioration and ground consolidation also significantly impact tunnel long-term behaviour (Di Murro et al., 2019; Li et al., 2015; Showkati et al., 2021; Usman and Galler, 2013; Yang et al., 2018b; Yoo, 2016). Usman and Galler (2013) found the mechanical deterioration of tunnel shotcrete increases load and deformation on the secondary lining, similar to Li et al. (2015), who noted greater surface settlement and tunnel deformation with severer hydraulic deterioration. Yoo (2016) observed hydraulic deterioration in tunnel drainage system increases tunnel internal forces and deformation. Distributed Fibre Optic Sensing (DFOS) strain measurements by Di Murro et al. (2019) and Di Murro (2019) showed an increasing deformation of a CERN tunnel due to both hydraulic and mechanical deteriorations. Showkati et al. (2021) found that primary support deterioration and ground weathering progressively increase lining axial thrust and bending moment.

In addition to the aforementioned factors, evolving environmental factors (e.g., rainfall and temperature) due to climate change and/or extreme weather events also significantly influence tunnel long-term performance (Arkell and Darch, 2006; Huibregtse et al., 2013; Jiang and Tan, 2021, 2022; Zhang et al., 2022). Many studies have highlighted the importance of these environmental factors. However, most of the focus has been on tunnel traffic disruptions and their socioeconomic impacts, as seen in Arkell and Darch (2006), Jiang and Tan (2021) and Jiang and Tan (2022). Limited efforts have been made to explore the effects of such climatic events, like rainfall and temperature variations, on the structural and mechanical responses of aging tunnels over the long term, let alone on discussing the underlying mechanisms behind such effects.

Regarding the thermal effect, several studies have found a direct correlation between temperature and tunnel structural deformation (Afshani et al., 2022; Bauduin and Kirstein, 2022; Du et al., 2021; Li et al., 2020; Tan et al., 2019; Yang et al., 2018a). Afshani et al. (2022) found that seasonal temperature variation causes cyclic opening and closing of tunnel segmental joints, and a similar pattern for tunnel convergence. This finding echoes the observation in Li et al. (2020) where seasonal temperature changes lead to repeated widening and shrinkage of tunnel joints, and subsequent changes in tunnel permeability and tunnel leakage volume. Monitoring results from Tan et al. (2019) found segmental joint openings decrease with rising temperature and pore water pressure. Similarly, Yang et al. (2018a) reported annual cyclic variations in lining strains and joint openings due to temperature and water level changes.

Bauduin and Kirstein (2022) also confirmed a direct correlation between tunnel lining joint movement and sinusoidal temperature curve. Most studies focused on joint opening in single segmental tunnels, with insufficient attention to whole tunnel circumferential behaviour. Conventional monitoring tools (e.g., wired strain gauges), limited by cabling and power requirements, restricts large-scale deployment around tunnel circumference, hindering comprehensive understanding of whole tunnel performance subject to thermal variation.

In terms of the rainfall effect, relevant studies have primarily focused on pore water pressure and groundwater table variations (Du et al., 2018; Fan et al., 2021; Fang et al., 2016; He et al., 2021; Li and Yuan, 2012; Ma et al., 2022; Zhang et al., 2022). Du et al. (2018) evaluated the impact of rainfall-induced pore water pressure and groundwater table change on tunnel stability. Fan et al. (2021) and Fang et al. (2016) used model tests to study the effect of surface rainfall recharge on tunnel performance and mechanical behaviour. He et al. (2021) concluded that heavy rainfall raises the water table and external groundwater pressure, increasing lining axial thrust and worsening structural soundness. Other studies by Li and Yuan (2012), Ma et al. (2022) and Zhang et al. (2022) instead focused on the effect of rainfall on the short-term response of tunnel structure during construction. Most studies mainly used model tests to simulate rainfall effects, emphasizing ground settlement and offering limited field measurements on long-term tunnel performance.

In summary, the review of previous studies identified three main research gaps regarding thermal and rainfall effects on tunnels: (1) too much highlight on the importance of the two effects but with rare dedicated analyses; (2) limited quantitative analyses based on field measurements; (3) scarce discussions on the underlying mechanisms behind the climatic factor-related tunnel performance variation. To address these research gaps and limitations, this research presents two case studies investigating the impact of rainfall and temperature on two aging tunnels through two innovative field monitoring systems. Section 2 examines the influence of seasonal rainfall on the long-term performance of two sections of CERN TT10 tunnel in Geneva using DFOS, while section 3 explores the effect of temperature on the long-term performance of a cross passage twin tunnel section of Dublin Port Tunnel (DPT) using wireless sensor network (WSN) monitoring. Section 4 summarises the findings on the hydraulic-thermal effects, providing references for the design, operation, and maintenance of, and bringing insights into the resilience of critical underground infrastructure vulnerable to climate change (e.g., increasing temperature), groundwater variations (e.g., geothermal operation, sea level rise, etc.) and other environmental factors.

2. CERN inclined tunnel: the impact of rainfall

2.1. TT10 tunnel and site description

CERN, located at the Swiss-French border, manages a 70km underground tunnel network housing the world's most powerful circular particle accelerator, as illustrated in Figure 1(a). These underground facilities, including caverns, shafts, and tunnels, were excavated in the highly weathered and heterogenous “red molasse” sedimentary rock of the Geneva basin. Over decades, lining cracks, water leakage and lining movement in some underground facilities have been observed. Of particular engineering concern is the TT10 tunnel, an inclined transfer tunnel connecting the beam accelerator of the PS to the SPS ring tunnels, as illustrated in Figure 1(b). Unlike the circular ring tunnels, the TT10 is a horseshoe-shaped tunnel constructed five decades ago with a diameter of 5.04m (for the circular part). It features a double lining of sprayed concrete and cast-in-situ concrete, with a standard waterproofing and drainage system, as shown in Figure 1(c).

The geology surrounding TT10 tunnel, the “red molasse” rock mass, consists of sequential layers of marls and sandstones from the Miocene tertiary period and by the diagenesis of Alpine detritus in a soft water basin (Fern et al., 2018). The geo-mechanical characteristics of the sub-horizonal interbedded rocks vary significantly, going from relatively stiff sandstones to weak marls (with considerable swelling potential for the very weak lumpy marl layers). The lumpy marl is the dominant rock strata intersecting the geological section at the location of major cracks, and it alters quickly when exposed to air and humidity, leading to losses of strength and even complete dis-integration (Parkin et al., 2002). Due to the compact structure of molasse, it normally has very low permeability of 10-09-10-10m/s, sometimes less than 10-10m/s (Di Murro, 2019; Xiao et al., 2020). Figure 2(a) shows TT10 tunnel geology profile based upon in-situ ground investigations, borehole logs, and face-logs. Due to structural deterioration, complex ground conditions, and tunnel inclination, severe defects were observed during inspections. Extensive compressive cracks at the tunnel crown, and longitudinal tensile cracks on the shoulders, as shown in Figure 2(b), were detected (Di Murro, 2019; Di Murro et al., 2019). Severe tunnel floor heaving and consequent crack widening pose significant risks to the serviceability and safety of the critical accelerator beamline, as seen in Figure 2(b). Groundwater ingress with calcite deposits and clogged drainage pipes at both sides of tunnel invert have been observed, indicating the build-up of external water pressure behind tunnel linings (Di Murro, 2019; Di Murro et al., 2019). All these defects demonstrate the ongoing deformation of TT10 tunnel, necessitating a long-term structural health monitoring system for tunnel condition assessment.

2.2. DFOS tunnel behaviour monitoring

To ensure the integrity of the accelerator beamline, a trial DFOS monitoring system based on Brillouin Optical Time-Domain Analysis (BOTDA) was deployed in two zones along TT10 tunnel in 2014 to monitor its long-term performance. Zone 1, with eight circumferential loops at an average depth of 25m (Figure 2(a) and Figure 3(a)), experienced intensifying lining cracks. Zone 2, with six loops at an average depth of 32m (Figure 2(a) and Figure 3(b)), was the most critical due to the majority of cracks. The number of tunnel cross-sectional loops in both zones is chosen to cover as many cracked areas as possible. The single-mode strain sensing fibre cables with a 9μm core were attached to TT10 tunnel lining using a hook-and-pulley system, with hooks screwed into liner, pullies attached to hooks and cables passing along pullies, as shown in Figure 3(c). The attachment illustrated in Figure 3(a) and (b) shows pre-strained cable section represented by solid line and loose/slack section by dash/dot line. After cable attachment, weights are applied to both ends for pretension, and glue is applied at the cable-pulley interface to fix the cables in place until the glue dries. At the end of the monitoring circuit, cable ends were joined in a connection box near a red access door (Figure 3(d)). The optical fibres were spliced to a standard extension cable and routed via a vertical shaft to a secure monitoring area housing the BOTDA unit (Di Murro, 2019). DFOS measurements were collected with a 1m spatial resolution and a 0.10m sampling interval for TT10 monitoring (Di Murro, 2019).

As the temperature within CERN's deep tunnels remains relatively constant at 26°C~27°C throughout the year and considering that the typically low thermal expansion coefficient of concrete fluctuates around 10με/°C or 10×10-06/°C (Di Murro, 2019; Yang et al., 2022), it is safe to conclude CERN tunnel performance is very unlikely to be influenced by ambient temperature variations, and therefore no temperature cable was deployed along strain cables. Another concern on gamma radiation affecting Brillouin scattering frequency of DFOS strain sensors was dismissed as the recorded gamma ray dose of 30Gy, well below the tolerance level of 100kGy for a single node fibre, barely induced any shift of strain measurement (Di Murro, 2019).

TT10 monitoring began in early 2015 after a baseline reading in late 2014, lasting until late 2017 (Di Murro et al., 2019). Strain readings were planned every 2-3 months but adapted to 3-4 months based on collected data and BOTDA unit availability. Incremental strains of TT10 liner were calculated by subtracting baseline measurements from progressive readings, resulting in 12 total measurements during the monitoring period (Di Murro, 2019; Di Murro et al., 2019).

2.3. Tunnel deformation and rainfall effect

A prior study by Di Murro et al. (2019) concluded that TT10 tunnel undergoes vertical elongation, with compressive strains at the crown and tensile strains at the sidewalls and arch corners (Figure 4). This case study, however, focuses on how tunnel deformation varies over time under the impact of rainfall events, detailed in the following subsections.

2.3.1 Rainfall, pore water pressure and groundwater level

To measure pore water pressure variations behind the tunnel lining, three piezometers (PZ 1-3) were installed behind a section of the Large Hydron Collider tunnel, as shown in Figure 1(b). Daily pore water pressures behind the tunnel lining were recorded by Source MeteoSwiss (IDAweb). Figure 5(a) shows the variation of daily rainfall and pore water pressure from June to October 2021. Generally, it seems it takes around a few days (e.g., 2/3 days) for pore water pressure to build up behind the liner after short-term heavy rainfalls, as evidenced by the delay between rainfall and pressure spikes in Figure 5 (e.g., heavy rainfall on August 6, 2021, followed by a pressure spike on August 8, 2021). This delay is due to a two-step rainwater infiltration process: the downward process of wetting front (ground saturation) and the rising of groundwater level (increasing pore water pressure) (Wang et al., 2020). With the cessation of heavy rainfall, the excess groundwater pressure finds its way into the tunnel drainage system gradually before it approximately levels off at a certain magnitude. For instance, after the August 8 spike, pressure gradually decreased over the following weeks without further rainfall. In addition to the fast increase of pore water pressure induced by short-term heavy rainfalls, continuous light rainfall also increases groundwater pressure, as seen in mid-July 2021 following continuous rainfall with an average

Accepted manuscript doi:
10.1680/jgeot.23.00074

of 8mm/day during a course of 6 days, demonstrating the cumulative effect of steady rainfall on pore water pressure. Therefore, after heavy rainfalls, pore water pressure behind tunnel linings is likely to increase. For permeable tunnels, the additional pore water pressure dissipates quickly but for impermeable tunnels with a clogged drainage system like TT10, the imposed groundwater

In drier months, pore water pressure acting on tunnel liner drops gradually with a decreasing rainfall, thus inducing a reduction in tunnel deformation.

The analysis above indicates that short-term rainfall events may lead to the short-term variation of pore water pressure in the local region (i.e., tunnel area). However, long-term variations in pore water pressure is more reliant on groundwater level change. To investigate the effect of rainfall on groundwater level and pore water pressure, Figure 5(b) shows groundwater and rainfall variations near the CERN TT10 tunnel from 2015 to 2017. Groundwater levels dropped in 2015, rose in early 2016, decreased in late 2016, and continuously increased in 2017. The changes in groundwater levels do not strictly follow rainfall patterns, suggesting influences from other sources like recharge from water body, lakes, snow, and glaciers (Zou et al., 2022), as illustrated in Figure 5(c). Therefore, in addition to rainfall, regional groundwater level variations arising from the above factors may also affect pore water pressure behind the tunnel lining. This indicates that seasonal pore water pressure changes are due to multiple factors, with rainfall being just one of them.

2.3.2 TT10 tunnel deformation development

Figure 6 shows the development of peak tensile and compressive strains over time in zone 1. Generally, both tensile and compressive strains experienced an increase over the monitoring duration, with notable periodic fluctuations each year. Figure 6(a) showed that tensile strains peaked in October 2015, November 2016, and October 2017, and troughed in March 2016 and February 2017, except for loop 4 possibly owing to human interference like cable bending/dislocation. Compressive strains in Figure 6(b) showed similar patterns, peaking around October and troughing around April each year. This demonstrates tunnel deformation increases in the second and third quarters and decreases in the first and fourth quarters each year, suggesting tunnel deformation fluctuates with season change. For this ageing tunnel, the generally increasing trend of lining deformation can be attributed to tunnel deterioration (evidenced by lining cracks and drainage system blockage) and surrounding rock mass deformation (e.g., calcite deposition into drainage system). Seasonal variation in lining strain is believed to be caused by seasonal changes in pore water pressure (behind tunnels) linked to seasonal rainfall, as there were no significant external disturbances, rather than tunnel deteriorations which typically do not cause periodic deformation as observed in Figure 6. This conclusion aligns with the finding from Wang et al. (2023).

As mentioned in section 2.3.1, seasonal pore water pressure variations are most likely linked to seasonal rainfall. Therefore, the observed seasonal and periodic fluctuations in tunnel deformation could be attributed to the effect of seasonal rainfalls. However, Figure 6 showed some inconsistencies in the proposed correlation between lining strain and rainfall. These inconsistencies arise because: (1) strain measurements are only affected by rainfall-related pore water pressure variations several days before each reading and long intervals between measurements may miss some significant groundwater pressure variations, partially contributing to the inconsistency; (2) groundwater pressure variations affecting tunnel strain come from not only seasonal precipitation but also other factors like water body recharge, ground permeability, and groundwater level changes, as illustrated in Figure 5(c) and concluded in section 2.3.1, further adding to the inconsistent correlation.

Similar to zone 1, DFOS measurements in zone 2 also show some seasonal fluctuation in liner strain, such as, troughs in March/April 2016 and peaks in November 2016 (as seen in Figure 7). However, the seasonal trends are less pronounced than in zone 1. The potential cause of this observation lies in the unfavourable geological conditions in zone 2, where weak lumpy marl (Figure 2(a)) plays a dominating role in causing the observed deformation, thus overshadowing the periodic strain variations induced by rainfall-related pore water pressure changes. This can be evidenced by the significant strains for loops 2 and 5, and the steadily increasing deformation in other loops.

2.3.3. Mechanism of TT10 tunnel deformation

Monitored strain measurements indicate that the steadily increasing tunnel deformation could be attributed to factors like tunnel deterioration and ground deformation, whilst the seasonal strain fluctuations are associated with changes in pore water pressure from rainfall events, as shown in Figure 5(a), when no significant external disturbances were observed. The coupling impact of rainfall-related pore water pressure variations and tunnel deteriorations like liner cracks and clogged drainage leads to the subsequent seasonal fluctuation in the steadily increasing tunnel strains as observed in CERN TT10 tunnel. Pore water pressure builds up with increasing rainfall, leading to higher stress and deformation in the liner, while the drop of rainfall implies the likely reduction of pore water pressure and associated decrease of lining strain and deformation. The rainfall-associated strain variation mechanism is also validated by numerical simulations. The detailed numerical model, boundary conditions, and modelling procedures are presented in Supplemental Materials S1. Numerical results confirmed that increasing rainfall gives rise to pore water pressure and lining strains, while decreasing rainfall leads to pressure dissipation and strain reduction, as seen in Figure S3. These results generally align with monitored trends in TT10 tunnel and therefore provide quantitative evidence on the rainfall-related seasonal tunnel structural performance, though they are preliminary and focus solely on rainfall-induced pore water pressure effect. Accurate and precise modelling requires detailed information on lining/ground deteriorations and monitored pore water pressure variations, but that falls out the scope of this study and specific efforts are thus needed to better represent the monitored TT10 performance. In addition to the general agreement, some inconsistencies in the rainfall-strain correlation observed in zone 1 could be linked to the missing of significant pore water pressure variations due to long strain measurement intervals and various sources of pore water pressure variations that affect lining strains, as described in section 2.3.2. The observed disagreements between strain and rainfall, in zone 2, were ascribed to the unfavourable weak lumpy marl layers that play a dominating role in causing the observed tunnel deformation, compromising the periodic strain variations induced by rainfall-related pore water pressure changes.

3. DPT twin tunnel: the impact of temperature

3.1. DPT and site description

Accepted manuscript doi: 10.1680/jgeot.23.00074

Dublin Port Tunnel was constructed firstly to alleviate problems including air pollution, traffic congestion and road safety concerns caused by Heavy Goods Vehicles frequently travelling within the city and secondly to provide better connectivity between Dublin Port and Dublin City. The 5.6km-long twin tunnel is structurally composed of four distinctive sections: northern and southern cut-and-cover sections (C&C), a middle bored section and one specific pipe-jacked section under the Dublin-Belfast railway line, as illustrated in Figure 8(a). Four vehicle cross passages (VCPs) (1km interval) and fifteen pedestrian cross passages (PCPs) (250m interval) were constructed for emergency use and evacuation. Geologically, the tunnel has the deepest stretch of up to 34m below ground at the mid-section and a gradual rise out to the ground level at both ends (Skipper et al., 2005), as shown in Figure 8(b). The northern and southern C&C sections traverse made ground, glacial sands and gravels, and glacial till (locally Dublin Boulder Clay), while the bored section is primarily in argillaceous calcisiltite (limestone). Structurally, bored tunnel section includes an annular shotcrete, a bolted pre-cast segmental lining and a cast-in-situ secondary lining. Hydraulically, waterproofing membranes were installed in-between three structural layers and drainage systems were constructed to aid the discharge of groundwater (Figure 8(c)). Groundwater drainage for the bored section flows towards the main sump buried underneath the invert of each bore at VCP 16 section, as illustrated in Figure 8(b). On opening in 2006, water ingress was found at several locations. Repairs comprised of replacing the waterproofing membranes and concrete locally. Subsequent inspections and maintenance works indicated ongoing lining deteriorations (e.g., lining cracks and water infiltration), especially around VCP 16 section (Figure 8(c)). To this end, a novel WSN system is adopted to monitor tunnel deformation and temperature in the long term, which is detailed below.

3.2. WSN tunnel performance monitoring

At VCP 16 section, 18 wireless sensor nodes (13 inclinometers, 2 crack-meters, 1 interface node and 2 gateways) were deployed to monitor lining structural changes and temperature variations, as shown in Figure 9(a). The micro-electromechanical system (MEMS) dual-axis tiltmeters, with temperature-measuring function and IP≥66 rating, were installed using a "drill-attach-level" method where bolts were drilled into linings followed by attaching the brackets and sensor nodes to the wall before adjusting them to level. The gateways, a key element of the monitoring system, are controlled and managed via remote wireless commands.

Figure 9 shows the onsite deployment of the sensors at four rings: 1) two central rings R2 and R3 intersecting VCP 16 opening, likely to develop the maximum displacement (Epel et al., 2021; Wu et al., 2020); 2) two rings R1 and R4, at a distance from VCP 16 opening, with more extensive cracks, water leakage and concrete spalling. The sensors were placed about 4m above the road surface to avoid possible destabilisation from maintenance washing (Figure 9(b)), with sensors T1, T4, T9, T10 and T13 at a height of around 4.20m from road surface and the nodes higher up at a height of around 6.00m (T2, T3, T5, T8, T11 and T12). Sensors T6 and T7 above the VCP 16 opening were installed at approximately 5.50m from the road surface.

3.3. Tunnel deformation and temperature effect

3.3.1 DPT deformation development

Accepted manuscript doi:
10.1680/jgeot.23.00074

Figure 10 shows the lining inclination development at sensing locations on tunnel rings R1, R2, R3 and R4 from April 2021 to June 2023. Positive inclinations mean anticlockwise rotation of tiltmeters while negative values mean clockwise rotation along tunnel circumference. Despite some variations, most inclination measurements show long-term development (e.g., T10), indicating ongoing tunnel deformation even after over a decade of operation without significant external disturbances (e.g., adjacent construction and surcharge loading). It should be noted that sensors T1 and T2 stopped functioning in March 2022 due to sensor data transmission unit failure, as shown by the omission of data from April 2022 onwards in Figure 10(a).

For ring R1, inclinations atT1, T2 and T3 increased from April to September 2021, then decreased until March 2022. After T1 and T2 stopped functioning, T3 showed another increase from April to August 2022 before another decrease until January 2023 and a further increase until June 2023. Accumulatively, the inclination development at T1, T2 and T3 on ring R1 during the monitoring generally remained counter clockwise. In contrast, the inclination development of T10, T11, T12 and T13 on R4 generally had an opposing trend (clockwise) as that on R1: a decrease from April-September 2021, an increase from September 2021 to January 2022, followed by another two decreases from January to August 2022 and January to June 2023, and another increase from September 2022 to January 2023, with the exception of T10 where the inclination variation reversed from September 2021 onwards. For R2 and R3, inclinations at T4 and T5 on R2 mirrored R1's counter-clockwise trend, while T6 showed clockwise rotation. Ring R3 inclinations (T7, T8, T9) generally developed clockwise. Figure 11(a) below from a prior study by Wang et al. (2023) illustrates the rates and tilting directions (curved red arrow) of the monitoring locations on the four rings. It can be seen the rotational movement for the monitoring locations on R1 and R4, R2 and R3 is generally symmetrical and the rates for T3, T10 and T11 on R1 and R4 are greater than the rates for other locations on R1 and R4 (T1, T2, T12 & T13) but the rates for T6 and T7 are smaller than that for other sensing locations on the same rings R2 and R3, respectively (T4, T5, T8 & T9). This observation, as concluded in Wang et al. (2023), is the result of two effects: (1) the effect of twin tunnel interaction that contributes to an approaching and symmetrical deformation of the twin-tunnel and enables a faster deformation rate for tunnel sections within the interaction zone; (2) the effect of vehicle cross passage (VCP) that causes a smaller rate for T6 and T7 which can be attributed to the pushback from VCP at layby-VCP conjunction area (strengthening/stiffening in lateral displacement responses at layby-VCP connection).

To better understand the magnitude of the monitored tunnel deformation, the prior studies by Wang et al. (2023) and Wang (2023) proposed a method to convert the monitored inclination data to convergence for DPT, as illustrated in Figure 12. Assuming the sensing location A0 on tunnel lining ring deforms to location A1 due to tunnel bending, and this deformation is accompanied by a rotation of $d\varphi$ and a movement of A0A1. In a polar coordinate system, the coordinates of point A0 before and after deformation are A0 (r, φ) and A1 $(r+dr, \varphi+ d\varphi)$ respectively. EA0 and EC are the tangent planes of the sensing location before and after bending. Line segment A0A1 is the total movement of point A0, and A0D and A1D are the horizontal and vertical components of the movement respectively. On the basis of geometrical derivation, the horizontal deformation of monitoring point A0 can therefore be

Accepted manuscript doi:
10.1680/jgeot.23.00074

obtained. The approach was based on assuming symmetrical tunnel lining bending, two-dimensional tunnel circumferential deformation that follows small displacement theory, and WSN inclinometer measurement equivalent to the rotation angle of the tangent plane of the monitoring location. The conversion of inclination to convergence is achieved via the following equation $dx=r\times\sin(d\varphi)\times\sin\varphi$ where the radius r and angle φ are measurable for each sensor location and dφ is the tilt data from WSN sensors (Wang, 2023; Wang et al., 2023).

The converted rate and direction of horizontal (solid blue arrow) and vertical deformation (hollow blue arrow) at different sensing locations are shown in Figure 11(b). The converted horizontal deformation from inclination data in Figure 10 ranges from 0.1355 to 0.3824 mm/year, comparable to previous studies such as 0.0425-0.2625mm/year for a CERN concrete tunnel (Di Murro, 2019), 0.085-0.125mm/year for a cast-iron tunnel in London Underground (Li et al., 2015; Soga et al., 2017), 0.06-0.12mm/year for a tunnel in Shanghai metro (Zhang et al., 2015), and 0.375mm/year in Afshani et al. (2022). Compared with the maximum convergence allowed for DPT, 0.2%D (D-tunnel diameter), these measurements fall well below the threshold, indicating the DPT tunnel's relatively stable behaviour over the monitoring period and its structural safety being within safe limits. For the observed increasing ongoing tunnel deformation, it is believed to be the result of tunnel deteriorations (Wang et al., 2023), and for the repeated annually cyclic increase and decrease of inclinations, it could be attributed to the effect of seasonal change where temperature and rainfall variations are potentially the two principal contributing factors, and more details are given in the following sections.

3.3.2 Mechanism of DPT temperature effect

3.3.2.1 Effect of temperature on DPT deformation

To study the correlation between temperature variation and lining deformation, it is firstly necessary to consider the bias drift of MEMS-based WSN sensors, where temperature can induce drift. Lab tests by the manufacturer showed a worst-case drift of 0.000125°/°C. With a maximum temperature variation of 10°C during the monitoring period, as observed in Figure 10, the maximum temperature-induced inclination drift is smaller than 0.00125°, which is reasonably negligible compared to the monitored inclinations. Figure 10 shows a clear correlation between tunnel's structural behaviour and seasonal temperature variation. For example, during warm seasons from April to August 2021 (spring and summer), inclinations increased by 0.0031°-0.0356° for T1, T2, T3, T4, T5, T8, T9 (anticlockwise) and decreased by 0.0155°-0.0225° for T6, T7, T10, T11, T12, T13 (clockwise). In cold seasons from September 2021 to January 2022 (autumn and winter), the trends reversed. Temperature decline caused a decrease in inclination ranging from 0.0001°~0.0166° for T1, T2, T3, T4, T5, T8, T9 (clockwise) and an increase within 0.0025°~0.0177° for T6, T7, T10, T11, T12 and T13 (anticlockwise). From February to April 2022 and from April to August 2022, the same trend was obtained, that is, this period witnessed an increase in inclination (0.0001°~0.0215°) for T3, T4, T5, T7, T9 (anticlockwise) and a decrease within (0.0045°~0.0302°) for T6, T8, T10, T11, T12 and T13 (clockwise). From September 2022 to June 2023, the annual cycle of inclination variation with temperature repeats. Though T1 and T2 stopped data transmission in March 2022, it may be predicted their inclination development likely followed the same seasonal pattern from April 2022 onwards.

Accepted manuscript doi:
10.1680/jgeot.23.00074

Figure 13 illustrates the correlation between inclination development and temperature variation during warm and cold seasons, where the numbering in legends (1, 2 and 3) means the first, second and third warm or cold season during the monitoring. In Figure 13(a) and (c), there is a "positive" correlation for R1 and R2 (except T6), where temperature increases lead to inclination increases, and vice versa. For example, T5's inclination increases with temperature during all three warm seasons monitored (April-August 2021, January-August 2022 and January-June 2023). However, in Figure 13(b) and (d), R3 and R4 shows a "negative correction, where inclinations increase as temperature decreases, with a few outliers. For instance, T6's inclination decreases with rising temperature during cold seasons (September 2021-January 2022 and September 2022-January 2023). Despite seasonal fluctuations (warm-season increase and cold-season decrease), Figure 10 also shows a gradual accumulation of tile over time.

To understand the temperature effect in a more straightforward way, Figure 14 illustrates tunnel deformation modes in both warm and cold seasons. Arc arrows represent rotational movement of monitored locations based on WSN sensor tilting, whilst inclination magnitudes indicate the changes of inclination during the selected warm (April-September 2021) and cold seasons (September 2021-January 2022) respectively. The solid red and dash blue lining shape represent the approximate tunnel deformation profiles during warm and cold seasons, respectively. During warm seasons, increased temperatures cause an increase in squatting deformation in the upper half of the tunnel rings (solid red curve and magnitude of inclination in Figure 14(a)). This deformation largely reverses during cold seasons as temperatures decrease (dashed blue curve in Figure 14(b)). The two-year monitoring data in Figure 10 suggests this seasonal deformation pattern repeats annually, in line with previous conclusions (Bauduin and Kirstein, 2022; Li et al., 2020). The mechanism behind these observations is detailed below.

3.3.2.2 Mechanism of DPT temperature effect

Results from the previous section show a clear correlation between structural inclination at VCP 16 in DPT and tunnel temperature variation. It is widely accepted that concrete is subject to heat-induced expansion and contraction stress caused by temperature variations (Wu et al., 2017) but such tunnel temperature variation-induced concrete volumetric change is largely considered elastic (Yang et al., 2018a), indicating the reversible nature of liner concrete expansion and contraction within tunnel ambient temperature setting. For VCP 16 section, ambient temperature increases in various warm seasons (April-August 2021, January-August 2022, and January-June 2023) lead to an increase in lining concrete thermal strain and subsequent thermal expansion, resulting in the observed increase in monitored tunnel deformation. In cold seasons (i.e., August 2021-January 2022 and August 2022-January 2023), temperature reduction induces concrete contraction, largely reversing the previous expansion and thus reducing tunnel deformation. Additionally, as mentioned earlier, the squatting deformation the tunnel concluded by Wang et al. (2023) is the result of twin tunnel interaction where the lateral stiffness of the surrounding ground (particularly the ground in-between) is smaller than the vertical stiffness due to (1) the short-term construction disturbance to the ground in between the twin tunnels causing the retraction of horizontal support from the middle ground to the twin tunnels (Epel et al., 2021; Laver et al., 2017; Li et al., 2015) and (2) the faster long-term deformation of the ground in between the twin tunnels than that of the ground at two sides of the twin tunnels. During periodic season changes, cyclic thermal changes, coupled with tunnel deteriorations, lead to seasonal and cumulative tunnel deformation, which subsequently could possibly alter internal forces, distort the lining, accelerate cracking, and eventually reduce bearing capacity of the lining. In turn, these events contribute to further tunnel deteriorations, such as the initiation of new lining cracks and propagation of existing ones, increasing water seepage and further decrease in liner bearing capacity, consequently causing time-dependent decline of tunnel serviceability with increasing lining deformation in the long term (Cui et al., 2020; Xu et al., 2022; Zhang et al., 2020b). To quantitatively understand the temperature effect, numerical simulations, with numerical model, material parameters, boundary conditions, mesh information, and modelling procedures detailed in Supplemental Materials S2 (Wang, 2023), were conducted, and results showed seasonal temperature variations induce seasonal deformation, and such deformation is largely reversible and elastic, as shown in Figure S5. These findings are consistent with field observations and thus in support of the mechanism of the temperature effect. It should be noted the results presented are just preliminary results arising from the effect of temperature only. The precise and accurate modelling of the observed tunnel performance and of the individual effect of temperature and lining deterioration requires the determination of detailed liner deterioration characteristics and the calculation of concrete and ground thermal properties based on lab tests. Thus, specific studies are required to better understand the coupling and individual effect of temperature and deterioration on tunnel performance.

The coupling of temperature, hydraulic (e.g., water seepage), and mechanical deteriorations (e.g., concrete crack and spalling) could result in long-term tunnel deformation: both thermal effect-caused reversible deformation and deterioration-induced irreversible deformation. For clarity, Figure 14(a) and Figure 14(b) graphically represent the tunnel deformation mode in cold and warm seasons, respectively. Unlike previous studies, the combined effect of temperature and deterioration presents a more comprehensive and accurate analysis on the long-term behaviour of ageing tunnels. The coupled influence of cyclic temperature variation and accumulated tunnel deteriorations increases tunnel deformation, but with elastic deformation reversing seasonally and plastic part accumulating over time. With time, the cumulative plastic displacements, if unmanaged, potentially may cause lining cracking, spalling, concrete peeling, joint separation, segment misalignment, waterproofing integrity compromise, water ingress and lining corrosion (Andreotti et al., 2020; Lu et al., 2024; Zhang and Zhao, 2024), and cause subsequent accelerated degradation and deterioration (Li et al., 2018). For the temperature-induced reversible tunnel displacements, they provide valuable data, insights and reference value to future tunnels whose performance is closely associated with temperature, such as geothermal energy tunnels (Barla and Di Donna, 2018).

3.3.3 Potential rainfall effect on DPT behaviour

To investigate the potential effect of precipitation on the long-term behaviour of DPT, rainfall data from the closest meteorology monitoring point was collected. Figure 15 shows the average monthly rainfall and structural inclination during the monitoring. The data indicate that (1) high rainfall volumes did not directly lead to significant variations in inclination; (2) substantial inclination changes were still recorded during months when rainfall volume remained similar. Therefore, it is reasonable to conclude that the structural performance of the monitored tunnel section does not have an apparent correlation with the average monthly rainfall near the tunnel.

Unlike CERN’s clogged drainage system, DPT's effective drainage system is to blame for the non-correlation between rainfall and DPT tunnel deformation as it prevents rainfall from significantly affecting the tunnel. DPT's drainage, including positive drains on secondary lining and normal drains behind both linings, effectively prevents the accumulation of groundwater pressures but instead dissipates them quickly through the drains. Consequently, rainfall variations do not significantly impact the development of DPT’s inclination as the strain variations in the CERN TT10 tunnel do. Thus, the rainfall effect exerts an insignificant impact on the structural performance of DPT cross passage twin tunnel, as supported by the results in Figure 15.

4. Conclusion

Tunnel long-term performance is influenced by various natural and anthropogenic factors, with temperature and rainfall being two major climatic influences that are often mentioned but rarely investigated in depth. Most previous studies on temperature effects focused on joint opening in single segmental tunnels, with insufficient attention on tunnel long-term circumferential performance, while rainfall studies largely concentrated on simulating ground settlement, lacking field data on tunnel structural performance. This paper presents two case studies on the hydro-thermal effects on two ageing tunnels’ long-term performance based on field measurements from two innovative monitoring systems: rainfall impact on CERN TT10 tunnel through spatially continuous strain monitoring by DFOS, and temperature effect on DPT via real-time WSN measurements. The quantitative analyses revealed the thermal-hydraulic impacts on ageing tunnel long-term performance in greater detail than previously available, with the main conclusions summarised as follows.

(1) DFOS continuous strain measurements showed a generally increasing deformation in CERN TT10 tunnel due to tunnel deterioration (lining cracks and drainage system blockage) and surrounding rock mass deformation (calcite deposition into drainage system). Seasonal variations in lining strain, with increases in the second and third quarters and decreases in the first and fourth quarters, are most likely linked to rainfall-related seasonal changes in pore water pressure, as evidenced by preliminary numerical results, rather than the result of tunnel deteriorations as lining degradations normally do not induce the observed periodicity in tunnel deformation.

(2) Inconsistencies in the proposed correlation between liner strains and rainfall variations in zone 1 could be attributed to two factors: (a) strain measurements are only affected by rainfall-related pore water pressure changes a few days before each reading, with long intervals between measurements missing some significant rainfall-related pore water pressure change, partially contributing to the inconsistency; (b) the assumed seasonal pore water pressure changes affecting lining strains arise not only from seasonal precipitation but also from other factors like water body recharge, ground permeability, and groundwater level changes, further adding to the inconsistent correlation. Upon comparison, the inconsistencies in zone 2 could be attributed to weak lumpy marls dominating tunnel deformation, overshadowing strain changes induced by rainfall-related pore water pressure variations.

Accepted manuscript doi: 10.1680/jgeot.23.00074

(3) Real-time WSN monitoring of DPT showed an overall growth in tunnel inclination with annual seasonal temperature variations. Unlike TT10, DPT's structural performance is primarily influenced by seasonal temperature changes. In warm months, inclination increased with temperature, while it decreased in cold months. Due to twin tunnel interaction, the twin tunnel squatted more and moved closer to each other at higher temperature but partially deformed back at lower temperature. In contrast, seasonal rainfall had an insignificant impact due to the effective drainage system controlling pore water pressure.

(4) DPT’s long-term deformation generally includes two components: thermal effect-caused reversible elastic deformation from lining concrete thermal expansion and contraction, and deterioration-induced irreversible plastic deformation from hydromechanical deterioration (e.g., leakage and cracking). Warm-season temperature increases cause thermal strain and expansion, leading to greater deformation, while cold-season temperature decreases cause contraction, largely but not completely reversing the expansion and thereby a decrease in deformation, as evidenced by preliminary numerical results. Under the coupled influence of tunnel deteriorations and annual cyclic temperature variations, the tunnel section further deteriorates, and the elastic deformation reverses back but plastic deformation accumulates with time, leading to the observed ongoing tunnel deformation in the long term.

In the aforementioned two case studies, both tunnels serve for routine operation subject to typical thermal and hydraulic variations. Such impact on tunnel deformation is found to be comparatively smaller than that caused by external disturbances and/or internal deterioration (e.g., adjacent construction, aged tunnel and ground erosion), but still plays an important role in tunnel long-term performance. During the life cycle of an underground infrastructure, it may encounter significant hydraulic and thermal variations induced by events and/or activities such as geothermal operation, significant and prolonged rainfall-caused pore water pressure change, sea level rise, climate change, etc. In this regard, research findings in this study can enhance the understanding of the long-term performance of critical underground infrastructure sensitive and vulnerable to seasonal variations in temperature, groundwater, and others, empowering infrastructure resilience and risk mitigation. In both case studies, there were some realistic and practical difficulties and restrictions challenging a comprehensive monitoring with sufficient sampling frequency, monitoring duration and spatial coverage, and it is anticipated that additional data from the resumption of CERN TT10 tunnel monitoring and continuous DPT monitoring, supported by additional models and/or analyses, may further enhance and strengthen the driving mechanisms behind the monitored observations. In this study, the quantitative evidence from the numerical results in support of the proposed seasonal effects is preliminary and more detailed simulations are needed in future studies to provide a more comprehensive understanding of these effects. Furthermore, how the monitored field data may inform the practical tunnel lining serviceability, durability, and/or even safety, such as the relation between field measurements and liner cracking, and how these influences may be mitigated, were only qualitatively but not quantitatively analysed. Addressing these issues, such as appropriate models and quantitative assessments, requires further extensive analyses that would be the scope of future studies through lab tests, model tests, numerical simulations and/more detailed monitoring.

Accepted manuscript doi: 10.1680/jgeot.23.00074

Acknowledgements
This work receives funding from various sources. The CERN TT10 tunnel monitoring was funded by Irish Research Council and EU Horizon 2020 research innovation programme under the Marie Skłodowska-Curie grant no. 713279 while Irish Centre for Research in Applied Geosciences of Science Foundation Ireland and Transport Infrastructure Ireland jointly funded the DPT monitoring project (13/RC/2092_P2). The authors would like to thank Prof. Kenichi Soga's research group (University of California, Berkeley) for their invaluable advice and assistance in the CERN tunnel project. Meanwhile, we also appreciate Prof. Mike Long's support (University College Dublin) for the DPT monitoring project and thank Geological Survey Ireland and Egis Road and Tunnel Operation for their contribution of DPT reports and data.

References

Afshani, A., Li, W., Oka, S., Itoh, Y., Akagi, H., 2022. Study of the long-term behavior of segmented tunnels in cohesive soil based on the circumferential joint opening. Tunnelling and Underground Space Technology 120, 104210.

Andreotti, G., Calvi, G.M., Soga, K., Gong, C., Ding, W., 2020. Cyclic model with damage assessment of longitudinal joints in segmental tunnel linings. Tunnelling and Underground Space Technology 103, 103472.

Arkell, B.P., Darch, G.J.C., 2006. Impact of climate change on London's transport network. Proceedings of the Institution of Civil Engineers - Municipal Engineer 159, 231-237.

Barla, M., Di Donna, A., 2018. Energy tunnels: concept and design aspects. Underground Space 3, 268-276.

Bauduin, C., Kirstein, A.A., 2022. Design, construction and monitoring of an underwater retaining wall close to an existing immersed tunnel. Tunnelling and Underground Space Technology 120, 104311.

Cui, S.a., Liu, P., Li, Z., Xu, X., Woody Ju, J., 2020. Shotcrete performance-loss due to seepage and temperature coupling in cold-region tunnels. Construction and Building Materials 246, 118488.

Di Murro, V., 2019. Long-term performance of a concrete-lined tunnel at CERN, Department of Engineering. University of Cambridge, Cambridge, UK.

Di Murro, V., Pelecanos, L., Soga, K., Kechavarzi, C., Morton, R., Scibile, L., 2019. Long-term Deformation Monitoring of CERN Concrete-lined Tunnels using Distributed Fibre-Optic Sensing. Geotechnical Engineering Vol. 50.

Du, B., Li, W., Tan, X., Ye, J., Chen, W., Sun, L., 2021. Development of load-temporal model to predict the further mechanical behaviors of tunnel structure under various boundary conditions. Tunnelling and Underground Space Technology 116, 104077.

Du, D., Dias, D., Yang, X., 2018. Analysis of earth pressure for shallow square tunnels in anisotropic and non-homogeneous soils. Computers and Geotechnics 104, 226-236.

Accepted manuscript doi:
10.1680/jgeot.23.00074

Epel, T., Mooney, M.A., Gutierrez, M., 2021. The influence of face and shield annulus pressure on tunnel liner load development. Tunnelling and Underground Space Technology 117, 104096.

Fan, H., Zhu, Z., Song, Y., Zhang, S., Zhu, Y., Gao, X., Hu, Z., Guo, J., Han, Z., 2021. Water pressure evolution and structural failure characteristics of tunnel lining under hydrodynamic pressure. Engineering Failure Analysis 130, 105747.

Fang, Y., Guo, J., Grasmick, J., Mooney, M., 2016. The effect of external water pressure on the liner behavior of large cross-section tunnels. Tunnelling and Underground Space Technology 60, 80-95.

Fern, E.J., Di Murro, V., Soga, K., Li, Z., Scibile, L., Osborne, J.A., 2018. Geotechnical characterisation of a weak sedimentary rock mass at CERN, Geneva. Tunnelling and Underground Space Technology 77, 249-260.

Guo, P., Liu, F., Lei, G., Li, X., Zhu, C.-w., Wang, Y., Lu, M., Cheng, K., Gong, X., 2021. Predicting Response of Constructed Tunnel to Adjacent Excavation with Dewatering. Geofluids 2021, 5548817.

He, B.-G., Zhang, Y., Zhang, Z.-Q., Feng, X.-T., Sun, Z.-J., 2021. Model test on the behavior of tunnel linings under earth pressure conditions and external water pressure. Transportation Geotechnics 26, 100457.

Hu, X., Bai, N., Li, H., 2008. Analysis on tunnel accident on Line 1 of Saint Petersburg Metro. Tunnel Construction 28, 418-422.

Huang, H.-w., Zhang, D.-m., 2016. Resilience analysis of shield tunnel lining under extreme surcharge: Characterization and field application. Tunnelling and Underground Space Technology 51, 301-312.

Huibregtse, J.N., Napoles, O.M., Dewit, M.S., 2013. Flooding of tunnels: quantifying climate change effects on infrastructure, The 11th International Conference on Structural Safety and Reliability. TNO Publications, New York.

Jiang, W., Tan, Y., 2021. Heavy rainfall-related excavation failures in China during 1994 to 2018: An overview. Engineering Failure Analysis 129, 105695.

Jiang, W., Tan, Y., 2022. Overview on failures of urban underground infrastructures in complex geological conditions due to heavy rainfall in China during 1994–2018. Sustainable Cities and Society 76, 103509.

Laver, R.G., Li, Z., Soga, K., 2017. Method to Evaluate the Long-Term Surface Movements by Tunneling in London Clay. Journal of Geotechnical and Geoenvironmental Engineering 143, 06016023.

Li, W., Afshani, A., Akagi, H., Oka, S., 2020. Influence of lining permeability and temperature on long-term behavior of segmented tunnel. Soils and Foundations 60, 425-438.

Accepted manuscript doi:
10.1680/jgeot.23.00074

Li, X., Li, C., Cao, W., Tao, M., 2018. Dynamic stress concentration and energy evolution of deep-buried tunnels under blasting loads. International Journal of Rock Mechanics and Mining Sciences 104, 131-146.

Li, X.G., Yuan, D.J., 2012. Response of a double-decked metro tunnel to shield driving of twin closely under-crossing tunnels. Tunnelling and Underground Space Technology 28, 18-30.

Li, Z., Soga, K., Wright, P., 2015. Long-term performance of cast-iron tunnel cross passage in London clay. Tunnelling and Underground Space Technology 50, 152-170.

Liang, R., Wu, J., Sun, L., Shen, W., Wu, W., 2021. Performances of adjacent metro structures due to zoned excavation of a large-scale basement in soft ground. Tunnelling and Underground Space Technology 117, 104123.

Liu, B., Zhang, D.-W., Yang, C., Zhang, Q.-B., 2020. Long-term performance of metro tunnels induced by adjacent large deep excavation and protective measures in Nanjing silty clay. Tunnelling and Underground Space Technology 95, 103147.

Lü, Q., Xiao, Z., Zheng, J., Shang, Y., 2018. Probabilistic assessment of tunnel convergence considering spatial variability in rock mass properties using interpolated autocorrelation and response surface method. Geoscience Frontiers 9, 1619-1629.

Lu, W., Song, S., Li, S., Liang, B., Li, J., Luan, Y., Wang, L., Sun, H., 2024. Study on mechanical properties of composite support structures in TBM tunnel under squeezing soft rock conditions. Tunnelling and Underground Space Technology 144, 105530.

Ma, E., Lai, J., Xu, S., Shi, X., Zhang, J., Zhong, Y., 2022. Failure analysis and treatments of a loess tunnel being constructed in ground fissure area. Engineering Failure Analysis 134, 106034.

Manchao, H., Leal e Sousa, R., Müller, A., Vargas, E., Ribeiro e Sousa, L., Xin, C., 2015. Analysis of excessive deformations in tunnels for safety evaluation. Tunnelling and Underground Space Technology 45, 190-202.

Meng, F.-y., Chen, R.-p., Xu, Y., Wu, K., Wu, H.-n., Liu, Y., 2022. Contributions to responses of existing tunnel subjected to nearby excavation: A review. Tunnelling and Underground Space Technology 119, 104195.

Shi, P., Li, P., 2015. Mechanism of soft ground tunnel defect generation and functional degradation. Tunnelling and Underground Space Technology 50, 334-344.

Showkati, A., Salari-rad, H., Hazrati Aghchai, M., 2021. Predicting long-term stability of tunnels considering rock mass weathering and deterioration of primary support. Tunnelling and Underground Space Technology 107, 103670.

Accepted manuscript doi: 10.1680/jgeot.23.00074

Skipper, J., Follett, B., Menkiti, C.O., Long, M., Clark-Hughes, J., 2005. The engineering geology and characterization of Dublin Boulder Clay. Quarterly Journal of Engineering Geology and Hydrogeology 38, 171-187.

Soga, K., Laver, R.G., Li, Z., 2017. Long-term tunnel behaviour and ground movements after tunnelling in clayey soils. Underground Space 2, 149-167.

Tan, X., Chen, W., Wu, G., Wang, L., Yang, J., 2019. A structural health monitoring system for data analysis of segment joint opening in an underwater shield tunnel. Structural Health Monitoring 19, 1032-1050.

Usman, M., Galler, R., 2013. Long-term deterioration of lining in tunnels. International Journal of Rock Mechanics and Mining Sciences 64, 84-89.

Wang, C., 2023. Monitoring and modelling the long-term performance of Dublin Port Tunnel, Civil, Structural and Environmental Engineering. University College Cork, Cork.

Wang, C., Friedman, M., Li, Z., 2023. Monitoring and assessment of a cross-passage twin tunnel long-term performance using Wireless Sensor Network (accepted). Canadian Geotechnical Journal.

Wang, F., Dai, Z., Takahashi, I., Tanida, Y., 2020. Soil moisture response to water infiltration in a 1-D slope soil column model. Engineering Geology 267, 105482.

Wu, D., Zhang, Y., Zhao, R., Deng, T., Zheng, Z., 2017. A coupled thermal-hydraulic-mechanical application for subway tunnel. Computers and Geotechnics 84, 174-182.

Wu, K., Cui, S., Liu, Y., Zhang, Q., Zhao, J., Zhang, Z., Han, Y., 2020. Study on the Mechanism of Grouting Under Different Tunnel Depth of Cross Passage. Geotechnical and Geological Engineering 38, 3291-3305.

Xiao, Z., Osborne, J.A., Perez-Duenas, E., Li, Z., 2020. The effect of pore water pressure on structural performance of CERN concrete-lined tunnel, Civil Engineering Research Ireland 2020, Cork, Ireland.

Xu, S., Ma, E., Lai, J., Yang, Y., Liu, H., Yang, C., Hu, Q., 2022. Diseases failures characteristics and countermeasures of expressway tunnel of water-rich strata: A case study. Engineering Failure Analysis 134, 106056.

Yang, J.-P., Chen, W.-Z., Li, M., Tan, X.-J., Yu, J.-x., 2018a. Structural health monitoring and analysis of an underwater TBM tunnel. Tunnelling and Underground Space Technology 82, 235-247.

Yang, L., Li, C., Luo, C., 2022. Thermal Strain Detection for Concrete Structure Cold Shrinkage under Stress Constraint with FBG. Sensors 22, 9660.

Yang, W., Baji, H., Li, C.-Q., 2018b. Time-dependent reliability method for service life prediction of reinforced concrete shield metro tunnels. Structure and Infrastructure Engineering 14, 1095-1107.

Yoo, C., 2016. Hydraulic deterioration of geosynthetic filter drainage system in tunnels – its impact on structural performance of tunnel linings. Geosynthetics International 23, 463-480.

Zhang, D.M., Ma, L.X., Zhang, J., Hicher, P.Y., Juang, C.H., 2015. Ground and tunnel responses induced by partial leakage in saturated clay with anisotropic permeability. Engineering Geology 189, 104-115.

Zhang, J., Liang, Y., Feng, T., 2020a. Investigation of the cause of shield-driven tunnel instability in soil with a soft upper layer and hard lower layer. Engineering Failure Analysis 118, 104832.

Zhang, J., Zhao, M., 2024. Experimental study on the mechanical properties of longitudinal joints of shield tunnels under large deformation conditions. Tunnelling and Underground Space Technology 144, 105447.

Zhang, Z., Huang, M., Pan, Y., Li, Z., Ma, S., Zhang, Y., 2022. Time-dependent analyses for ground movement and stress field induced by tunnelling considering rainfall infiltration mechanics. Tunnelling and Underground Space Technology 122, 104378.

Zhang, Z., Sun, F., Chen, B., 2020b. Thermo–mechanical coupled analysis for tunnel lining with circular openings. Tunnelling and Underground Space Technology 102, 103409.

Zheng, G., Su, Y., Diao, Y., Zhao, Y., Chen, H., Huang, J., 2022. Field measurements and analysis of real-time capsule grouting to protect existing tunnel adjacent to excavation. Tunnelling and Underground Space Technology 122, 104350.

Zou, Y., Kuang, X., Feng, Y., Jiao, J.J., Liu, J., Wang, C., Fan, L., Wang, Q., Chen, J., Ji, F., Yao, Y., Zheng, C., 2022. Solid Water Melt Dominates the Increase of Total Groundwater Storage in the Tibetan Plateau. Geophysical Research Letters 49, e2022GL100092.

Accepted manuscript doi:
10.1680/jgeot.23.00074

Figure captions

Fig. 1. Location of CERN and TT10 tunnel

Fig. 2 .TT10 tunnel geology and deteriorations (Di Murro, 2019)

Fig. 3. DFOS instrumentation details in TT10 tunnel (Di Murro, 2019; Di Murro et al., 2019)

Fig. 4. Illustration of CERN TT10 tunnel deformation mode (Di Murro et al., 2019)

Fig. 5. Groundwater pressure, groundwater level and rainfall development over time

Fig. 6. Strain and rainfall variation over time in zone 1 (strain data from Di Murro (2019))

Fig. 7. Strain and rainfall variation over time in zone 2 (strain data from Di Murro (2019))

Fig. 8. DPT location and site conditions

Fig. 9. WSN sensor deployment at VCP 16 section

Fig. 10. DPT inclination and temperature development with time (monthly average)

Fig.11. Monitored inclination and converted convergence of the monitored DPT section (reedited from Wang et al. (2023) and Wang (2023))

Fig. 12. Inclination-convergence model for non-segmental DPT (Wang, 2023)

Fig. 13. Correlation between monitored inclination and temperature

Fig. 14. Effect of temperature on DPT twin tunnel deformation mode (illustration only)

Fig. 15. DPT inclination and rainfall development with time (monthly average)

Accepted manuscript doi:
10.1680/jgeot.23.00074

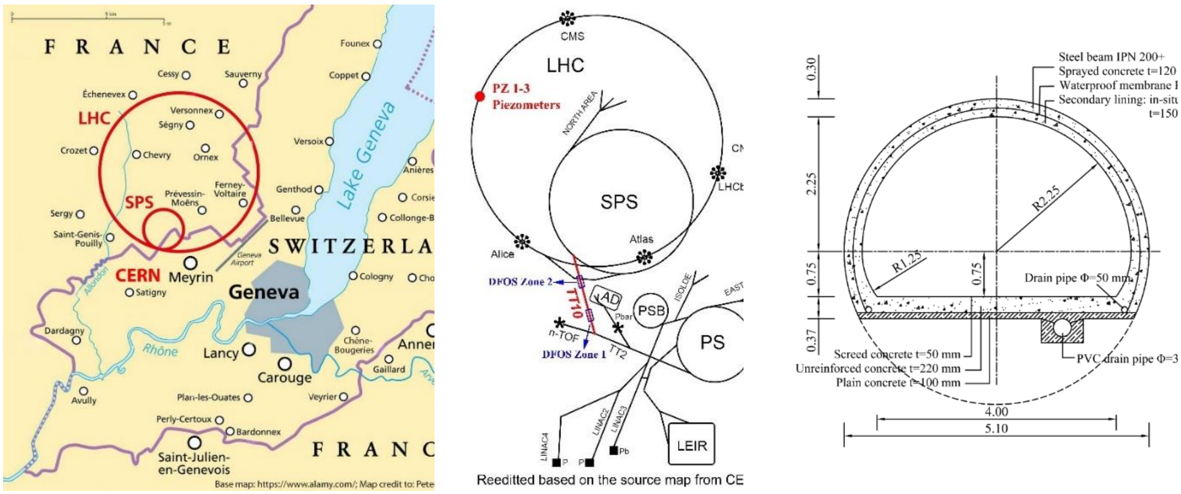

(a) CERN at the Swiss-French border

(b) TT10 tunnel location

(c) TT10 tunnel cross section

Figure 1

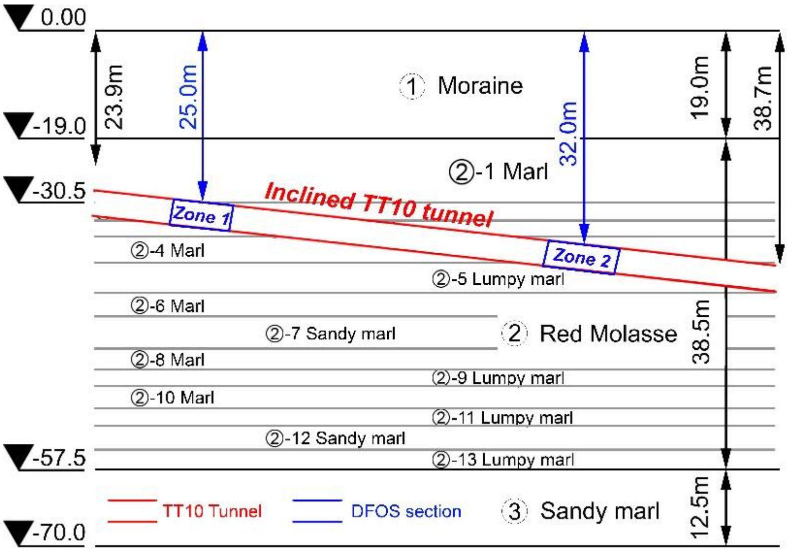

(a) Geology around one section of TT10 tunnel

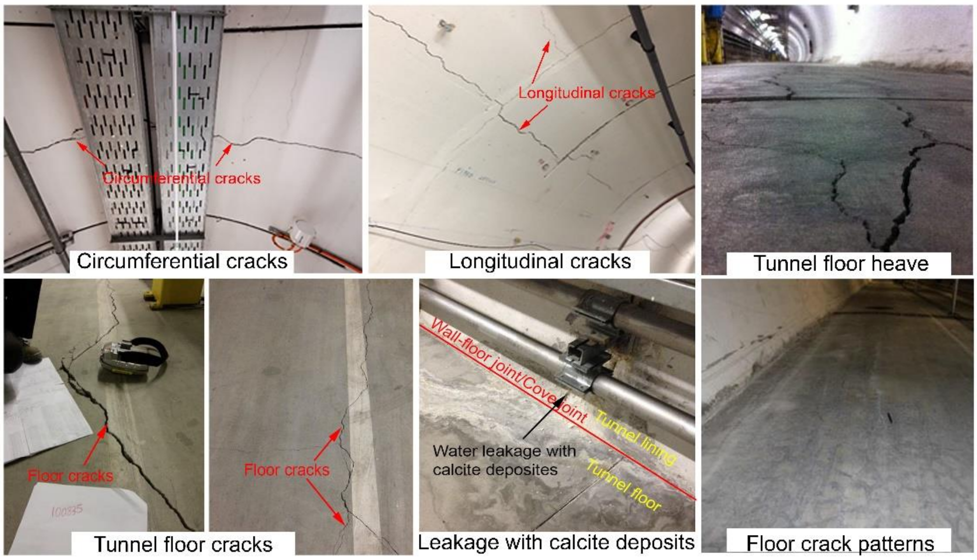

(b) TT10 tunnel deteriorations

Figure 2

Accepted manuscript doi:
10.1680/jgeot.23.00074

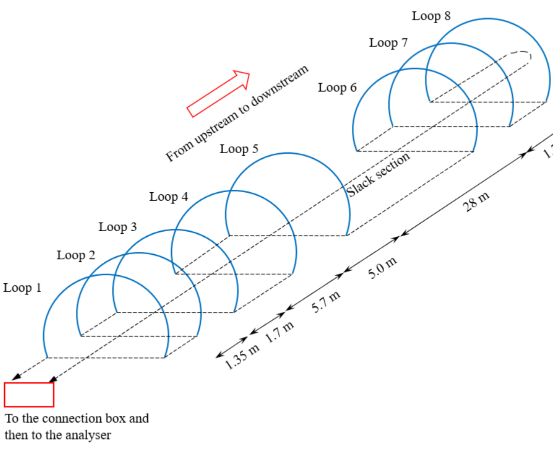

(a) Zone 1 DFOS deployment

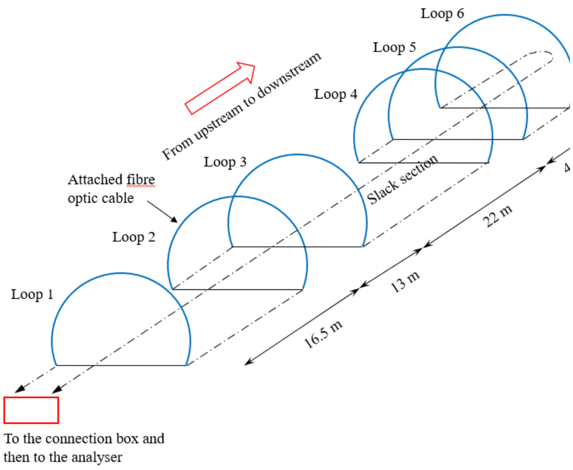

(b) Zone 2 DFOS deployment

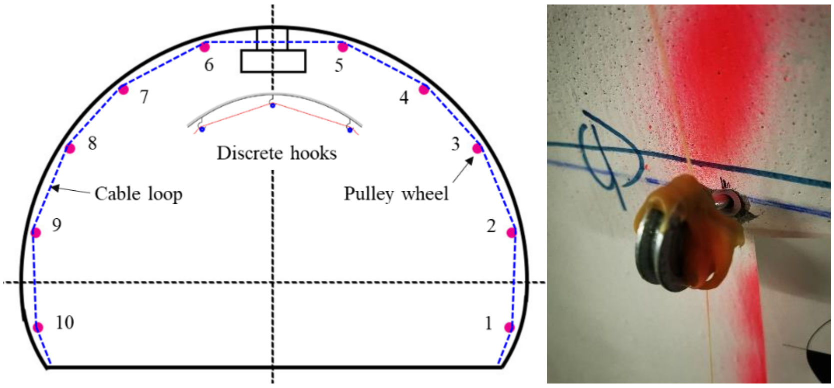

(c) Illustration of the circumferential cable loop and hook-pully system

(d) DFOS onsite deployment, cable connection box and BOTDA

Figure 3

Accepted manuscript doi:
10.1680/jgeot.23.00074

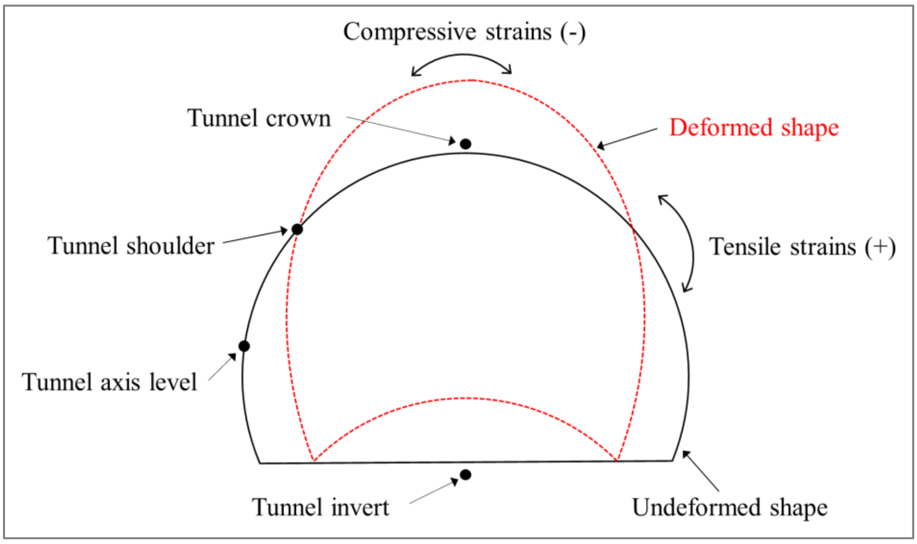

Figure 4

Accepted manuscript doi:
10.1680/jgeot.23.00074

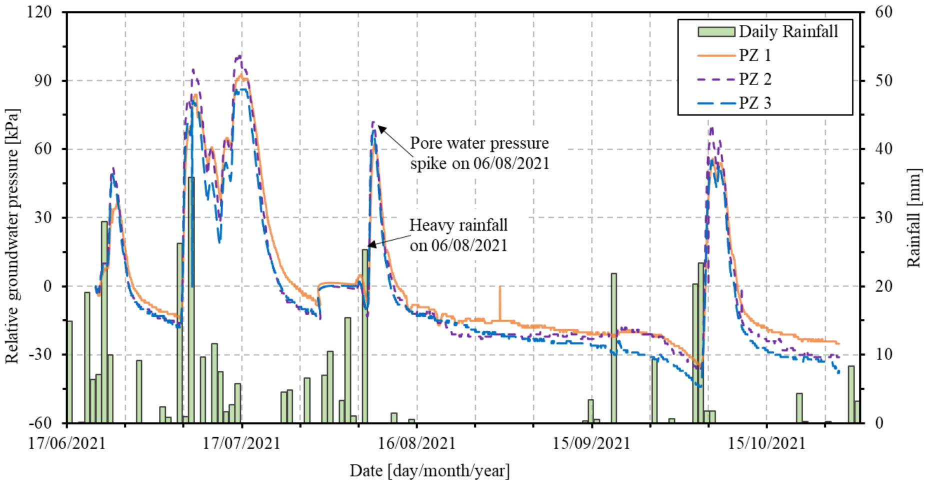

(a) Groundwater pressure and rainfall variation from June to October 2021 (daily average)

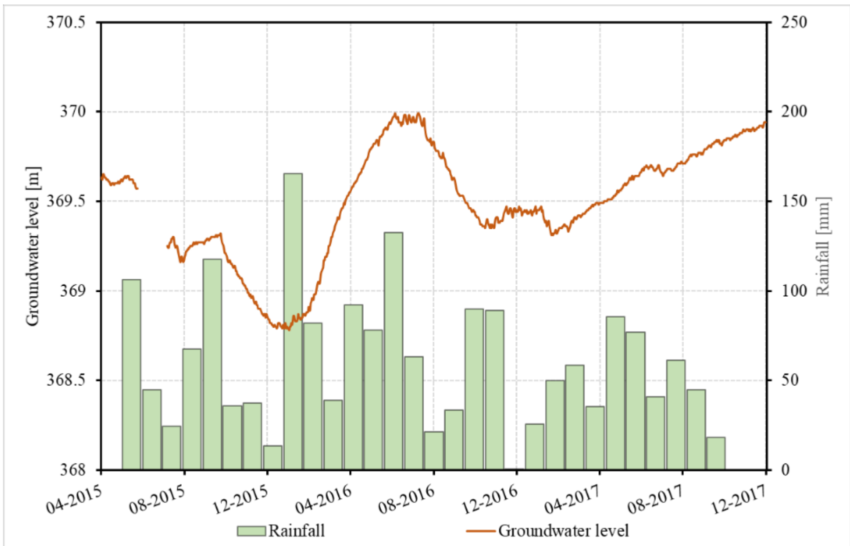

(b) Groundwater level and rainfall development from 2015 to 2017 (monthly average)

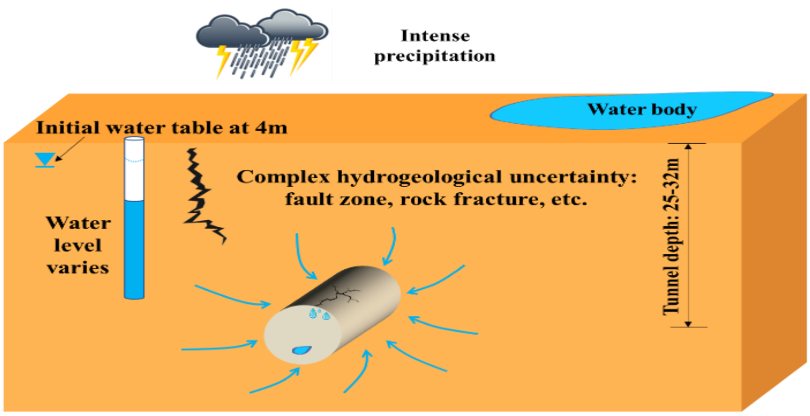

(c) Illustration of rainfall and groundwater pressure

Figure 5.

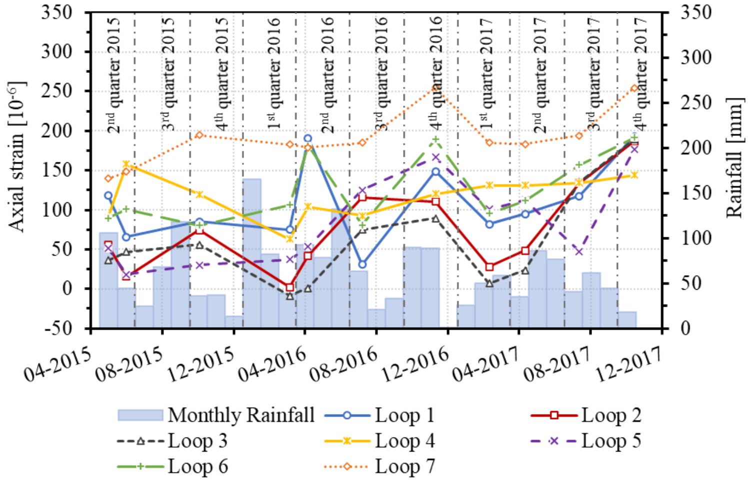

(a) tensile strain and rainfall variation with time

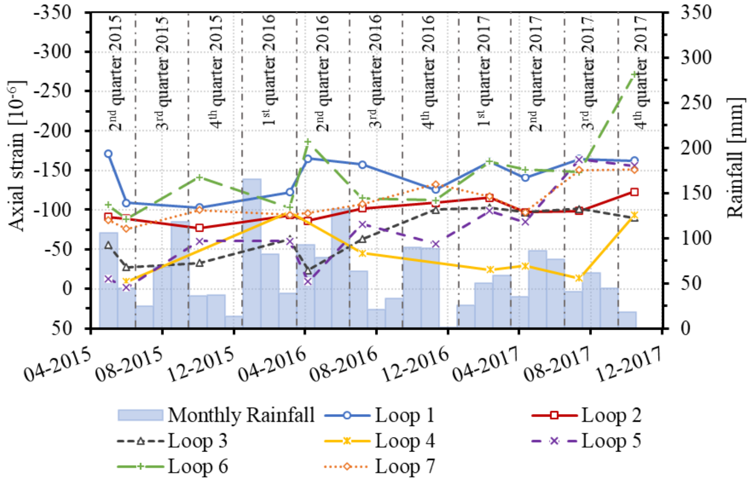

(b) compressive strain and rainfall variation with time

Figure 6

Accepted manuscript doi:
10.1680/jgeot.23.00074

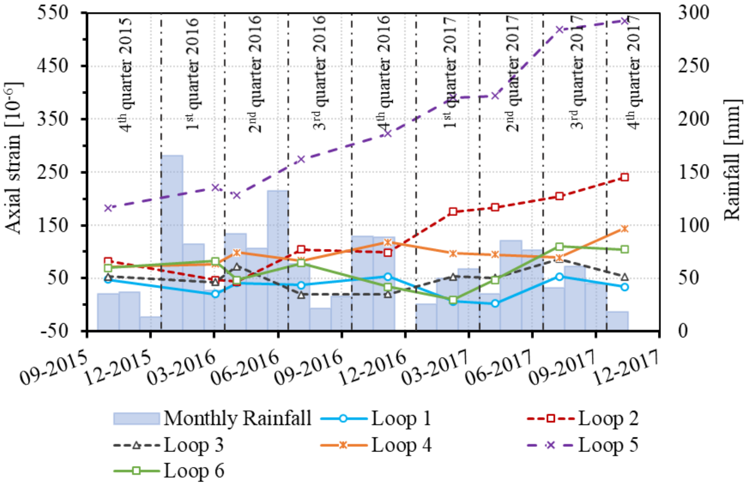

(a) tensile strain and rainfall variation with time

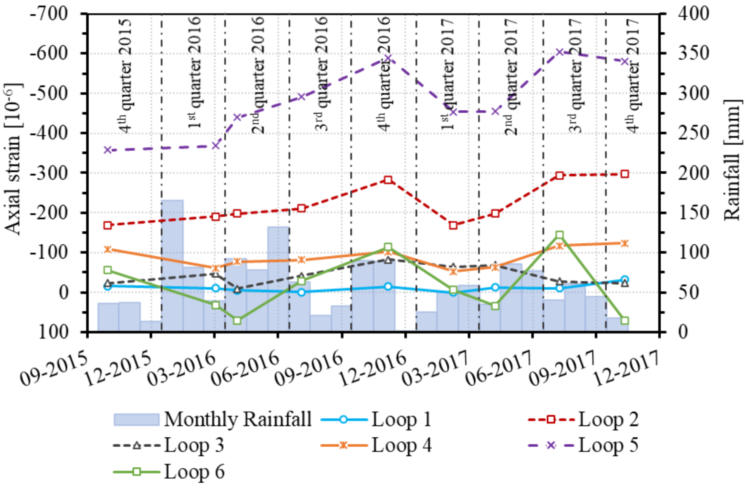

(b) compressive strain and rainfall variation with time

Figure 7

Accepted manuscript doi:
10.1680/jgeot.23.00074

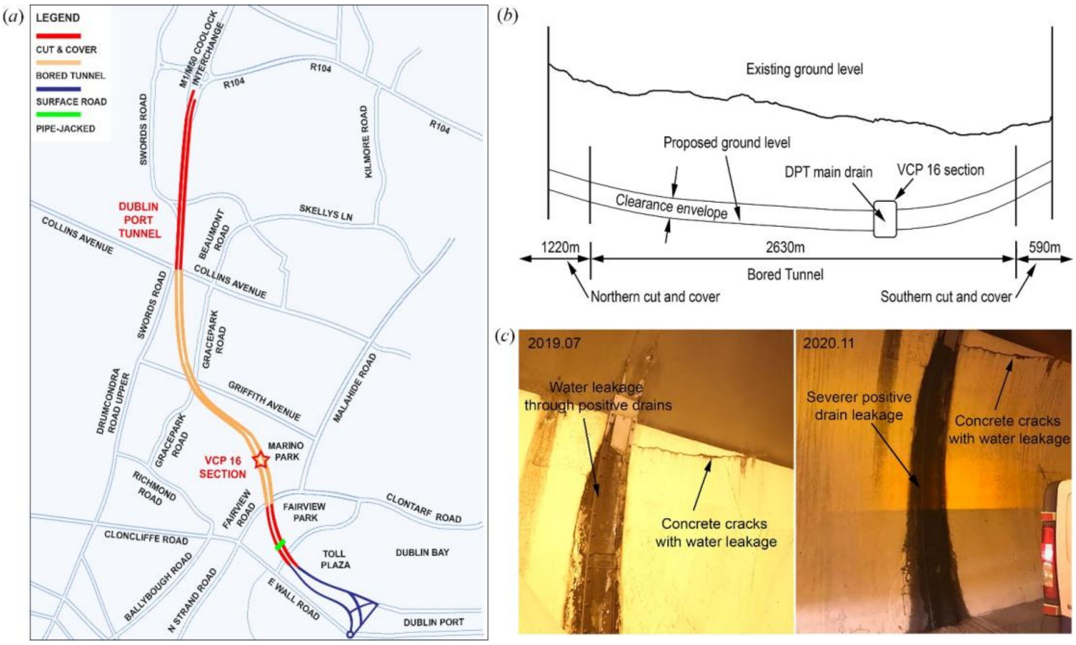

Figure 8

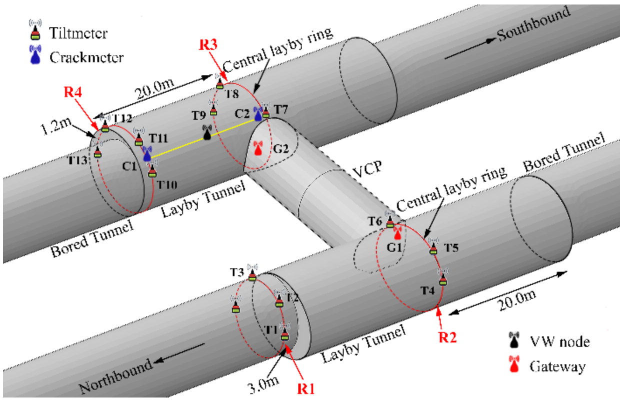

(a) Sensor deployment illustration

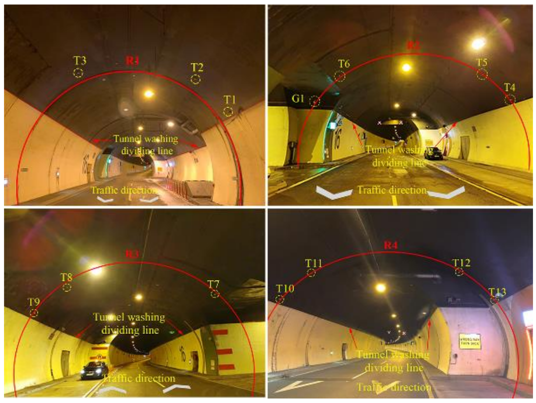

(b) Onsite sensor deployment

Figure 9

Accepted manuscript doi:
10.1680/jgeot.23.00074

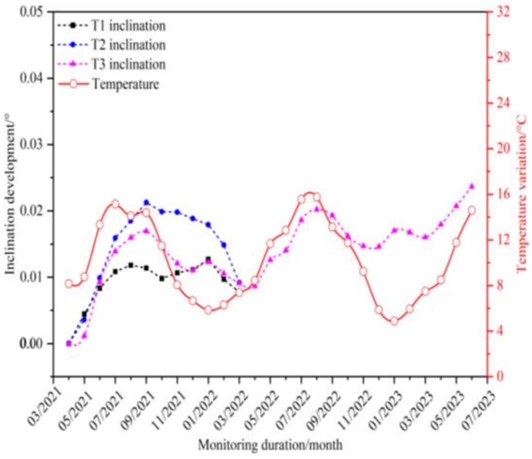

(a) R1 inclination & temperature development

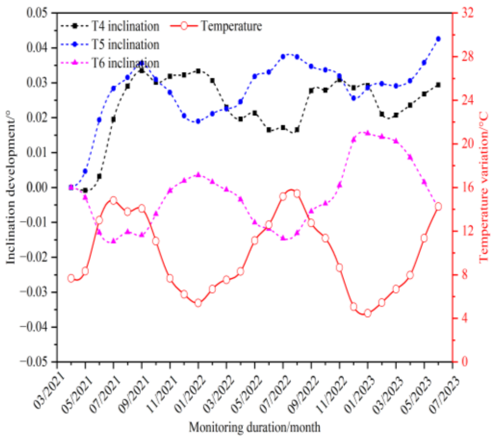

(b) R2 inclination & temperature development

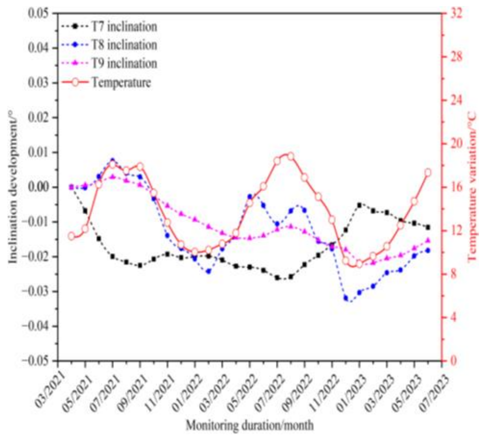

(c) R3 inclination & temperature development

Accepted manuscript doi:
10.1680/jgeot.23.00074

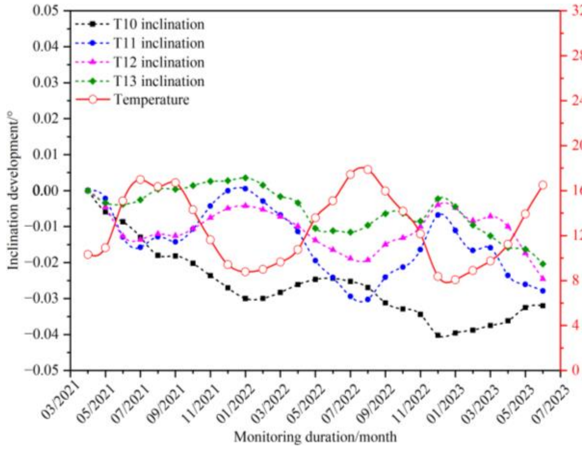

(d) R4 inclination & temperaturedevelopment

Figure 10

Accepted manuscript doi:
10.1680/jgeot.23.00074

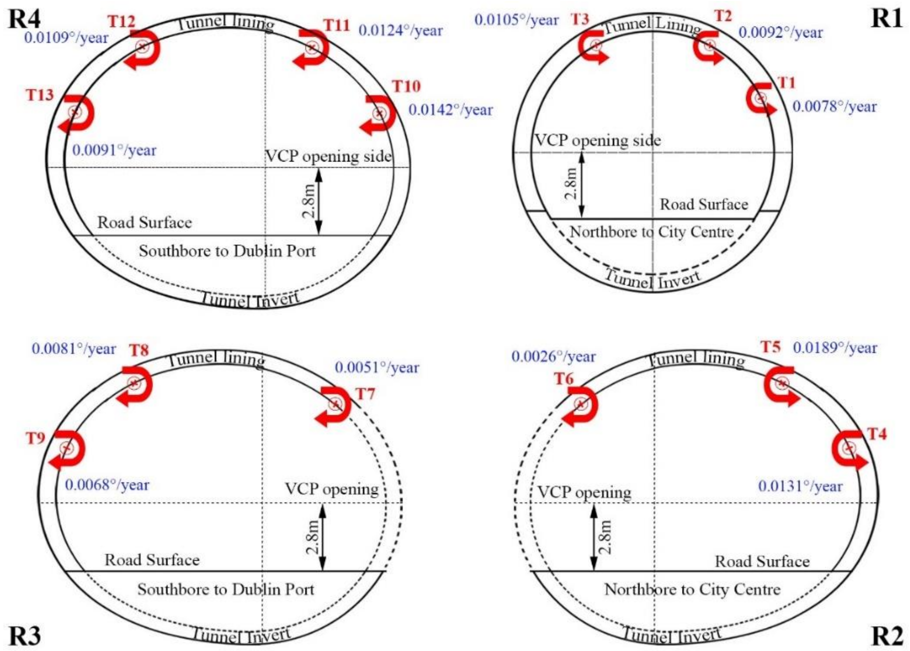

(*a*) Rate and tilting direction of inclination at sensing location

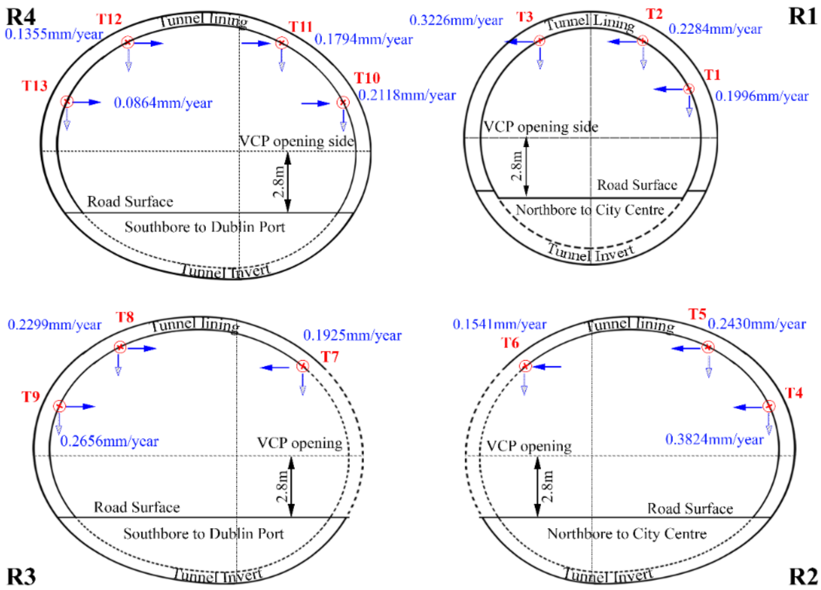

(b) Rate and direction of horizontal and vertical deformation at sensing locations

Figure 11.

Accepted manuscript doi:
10.1680/jgeot.23.00074

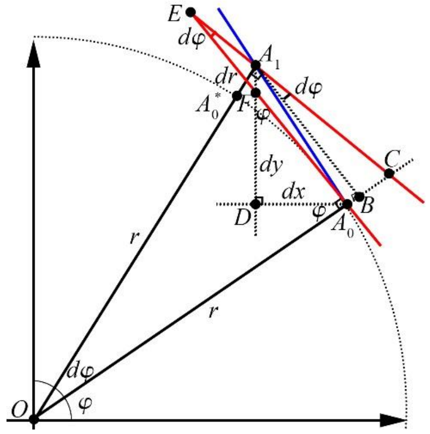

Figure 12

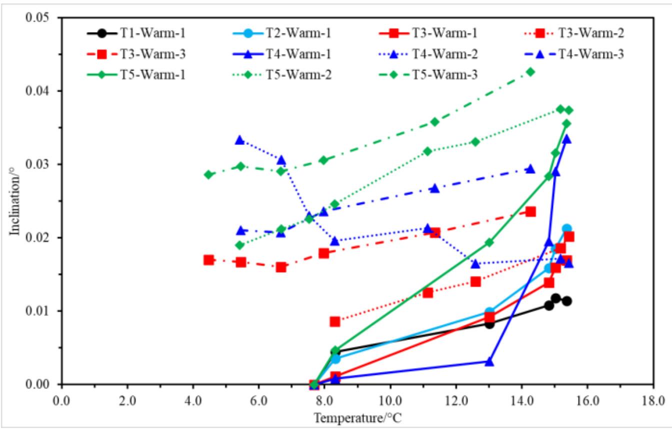

(a) “Positive” correlation in warm seasons

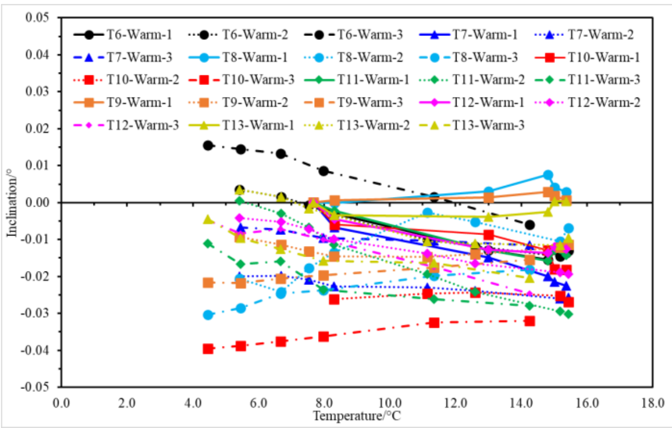

(b) “Negative” correlation in warm seasons

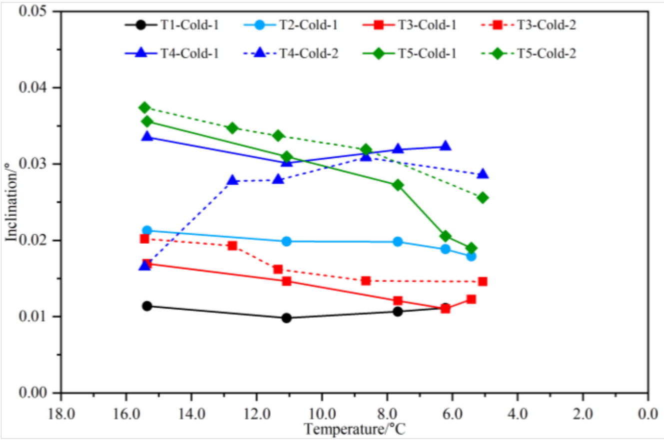

(c) "Positive" correlation in cold seasons

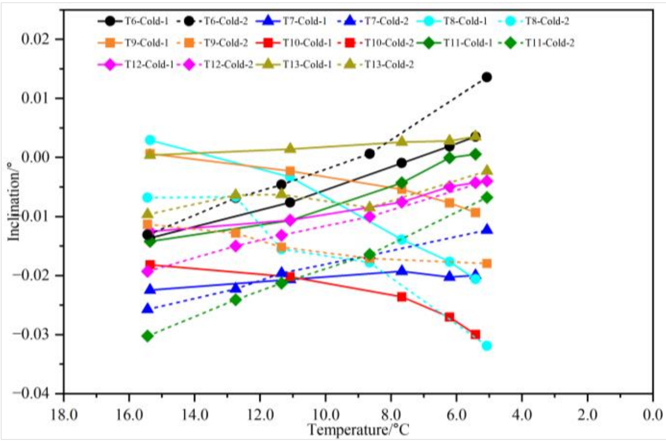

(d) "Negative" correlation in cold seasons

Figure 13

Accepted manuscript doi:
10.1680/jgeot.23.00074

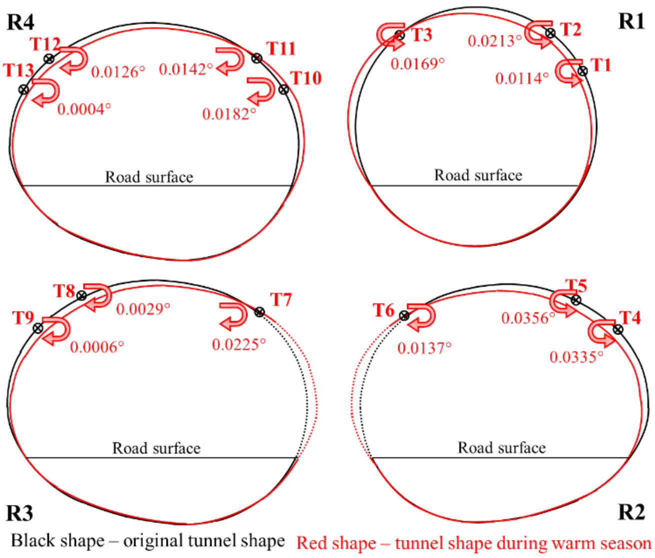

(a) Tunnel deformation mode in warm season

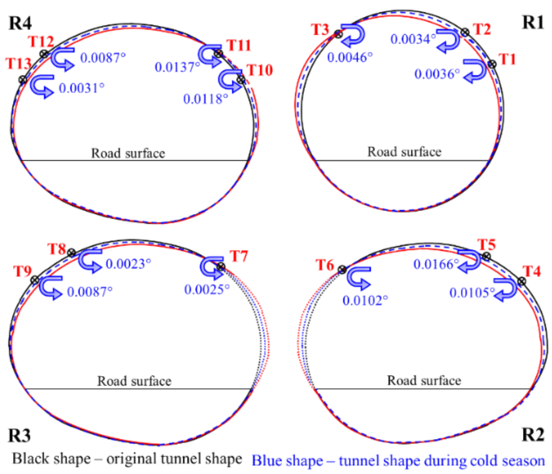

(b) Tunnel deformation mode in cold season

Figure 14

Accepted manuscript doi:
10.1680/jgeot.23.00074

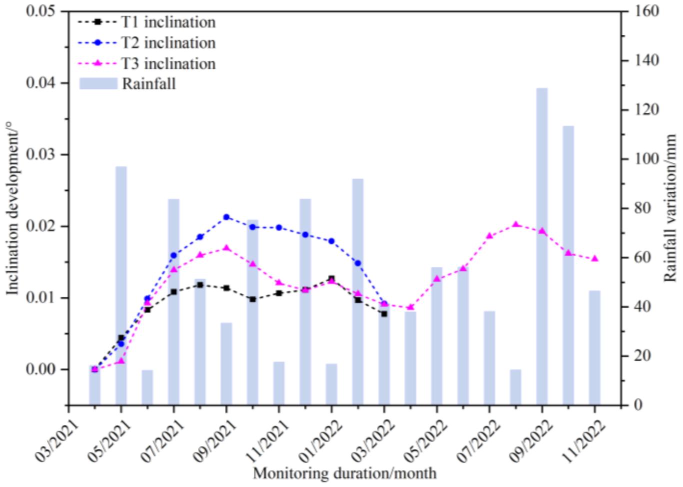

(a) R1 inclination & rainfall development

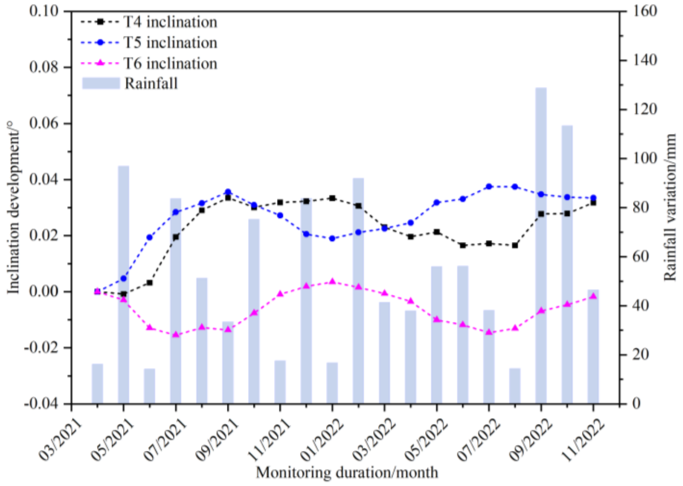

(b) R2 inclination & rainfall development

Accepted manuscript doi:
10.1680/jgeot.23.00074

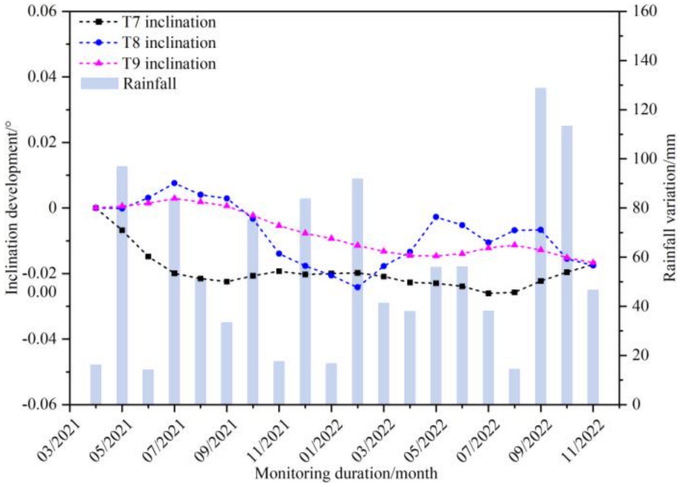

(c) R3 inclination & rainfall development

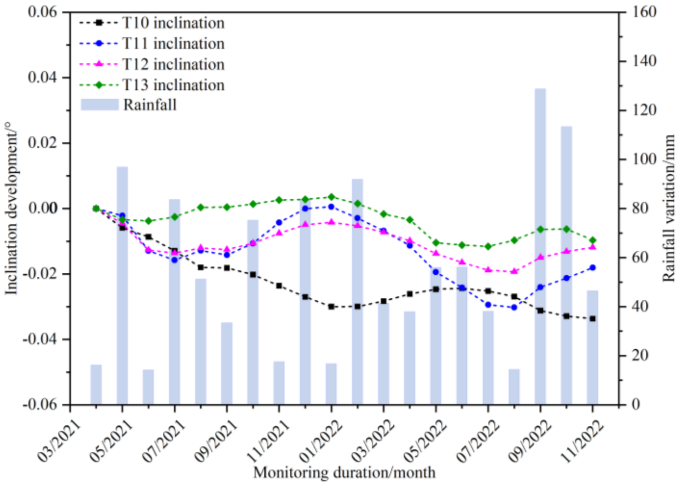

(d) R4 inclination & rainfall development

Figure 15